Bone 118 (2019) 89–98

Contents lists available at ScienceDirect

Bone

journal homepage: www.elsevier.com/locate/bone

Characterization of the bone marrow adipocyte niche with three-dimensional electron microscopy

Hero Robles [a], SungJae Park [a], Matthew S. Joens [d], James A.J. Fitzpatrick [b,c,d,e], Clarissa S. Craft [a,b], Erica L. Scheller [a,b,*]

[a] Division of Bone and Mineral Diseases, Department of Medicine, Washington University, St. Louis, MO, USA
[b] Department of Cell Biology & Physiology, Washington University, St. Louis, MO, USA
[c] Department of Neuroscience, Washington University, St. Louis, MO, USA
[d] Center for Cellular Imaging, Washington University, St. Louis, MO, USA
[e] Department of Biomedical Engineering, Washington University, St. Louis, MO, USA

ARTICLE INFO

Article history:
Received 15 December 2017
Revised 12 January 2018
Accepted 15 January 2018
Available online 31 January 2018

Keywords:
Bone marrow
Ultrastructure
Adipocyte
Fat
Hematopoiesis
Erythropoiesis
Anemia
Bone marrow adipose tissue

ABSTRACT

Unlike white and brown adipose tissues, the bone marrow adipocyte (BMA) exists in a microenvironment containing unique populations of hematopoietic and skeletal cells. To study this microenvironment at the subcellular level, we performed a three-dimensional analysis of the ultrastructure of the BMA niche with focused ion beam scanning electron microscopy (FIB-SEM). This revealed that BMAs display hallmarks of metabolically active cells including polarized lipid deposits, a dense mitochondrial network, and areas of endoplasmic reticulum. The distinct orientations of the triacylglycerol droplets suggest that fatty acids are taken up and/or released in three key areas – at the endothelial interface, into the hematopoietic milieu, and at the bone surface. Near the sinusoidal vasculature, endothelial cells send finger-like projections into the surface of the BMA which terminate near regions of lipid within the BMA cytoplasm. In some regions, perivascular cells encase the BMA with their flattened cellular projections, limiting contacts with other cells in the niche. In the hematopoietic milieu, BMAT adipocytes of the proximal tibia interact extensively with maturing cells of the myeloid/granulocyte lineage. Associations with erythroblast islands are also prominent. At the bone surface, the BMA extends organelle and lipid-rich cytoplasmic regions toward areas of active osteoblasts. This suggests that the BMA may serve to partition nutrient utilization between diverse cellular compartments, serving as an energy-rich hub of the stromal-reticular network. Lastly, though immuno-EM, we've identified a subset of bone marrow adipocytes that are innervated by the sympathetic nervous system, providing an additional mechanism for regulation of the BMA. In summary, this work reveals that the bone marrow adipocyte is a dynamic cell with substantial capacity for interactions with the diverse components of its surrounding microenvironment. These local interactions likely contribute to its unique regulation relative to peripheral adipose tissues.

1. Introduction

In biology, structure and function are inexorably linked. Post-world war II, technological advancements brought high-resolution transmission electron microscopy into the laboratory, facilitating a renaissance of structural observations which have since informed our understanding of adipocyte function. In addition to defining the subcellular characteristics of peripheral white adipose tissue (WAT) adipocytes [1–6], work by Loncar et al. from 1987 to 1991 [2–4] identified and characterized what we currently refer to as beige [7] or BRITE [8] adipocytes. As with more recent studies [9], Loncar discovered that these multilocular, mitochondria-rich fat cells accumulated in small mammals after cold exposure [2–4].

Around the same time, Tavassoli undertook the first electron microscopic characterization of the bone marrow adipocyte (BMA) [10,11]. His work revealed that the BMA is ultrastructurally similar to WAT with three key distinctions. First, while the WAT adipocyte has been described as being 'embraced' by a network of collagen fibers [6], the bone marrow adipose tissue (BMAT) adipocyte lacks a collagen support system [10,11]. Second, vacuoles were notable in the lipid droplet during BMAT, but not WAT, adipocyte maturation [10,11]. Third, BMAs did not accumulate glycogen during development [11]. It was also noted

Abbreviations: BMA, bone marrow adipocyte; BMAT, bone marrow adipose tissue; EM, electron microscopy; FIB-SEM, focused ion beam scanning electron microscopy; WAT, white adipose tissue; PBS, phosphate buffered saline.

* Corresponding author at: Division of Bone and Mineral Diseases, Department of Internal Medicine, Washington University, BJCIH Rm 11609, 425 S. Euclid Ave, Saint Louis, MO 63110, USA.
E-mail addresses: hrobles@wustl.edu (H. Robles), sungjaepark@wustl.edu (S. Park), mjoens@wustl.edu (M.S. Joens), fitzp@wustl.edu (J.A.J. Fitzpatrick), clarissa.craft@wustl.edu (C.S. Craft), scheller@wustl.edu (E.L. Scheller).

https://doi.org/10.1016/j.bone.2018.01.020
8756-3282/

that the development of the BMA is much slower than adipocytes in WAT, which may account for the reduced glycogen deposits [11]. A comparison of the known ultrastructural features of white, beige, and bone marrow adipocytes is summarized in Table 1.

Despite its histologic and ultrastructural similarity to the WAT, both recent and historic work reveals that the function and regulation of BMAT is often unique (reviewed in Scheller et al. [12,13]). For example, BMAs counterintuitively accumulate with chronic caloric restriction while WAT is lost [14–16]. By contrast, unlike WAT, BMAT responds readily to experimentally-induced anemia by depletion of its intracellular lipid stores [17,18]. We hypothesize that this is mediated, at least in part, by its distinct microenvironmental context. With the advent of focused ion beam scanning electron microscopy (FIB-SEM), we are now able to study cells within their native microenvironment in three-dimensions at nanoscale resolution. Our study uses this technology to further explore the interactions between BMAs and cells within the hematopoietic and skeletal niche, revealing novel relationships and informing our understanding of BMAT function within bone.

2. Materials and methods

2.1. Animals

All animal procedures were approved by the animal use and care committee at Washington University (Saint Louis, MO, USA). Animals were housed at 22 °C on a 12-hour light/dark cycle with daily care by the Division of Comparative Medicine.

2.2. FIB-SEM sample preparation, scanning, and dataset information

2.2.1. Sample preparation protocol #1

Two datasets were generated with this protocol: (Dataset #1, Figs. 1–5, Supplementary Figs. 1–2) C57BL/6 J mouse proximal tibial metaphysis, 1329 serial electron micrographs and (Dataset #2, Fig. 6) C57BL/6 J mouse tail vertebrae, 967 serial electron micrographs. An adult male C56BL6/J mouse (Jackson Labs Stock: 000664) was sedated with ketamine/xylazine and perfused with 10 mL saline followed immediately by 10 mL of fixative cocktail (0.15 M cacodylate buffer, 2.5% glutaraldehyde, 1.25% paraformaldehyde (PFA), and 2.3% picric acid). The tibia and C3 tail vertebrae were isolated and post-fixed overnight at 4 °C. Tissues were washed in water for 30-min prior to decalcification in 14% EDTA, pH 7.4 for 3-days at 4 °C with daily changes of EDTA. A fresh razor blade was used to section the tibia horizontally to isolate the proximal metaphysis. The C3 tail vertebrae was processed in the same way to isolate the middle third. Decalcified tissues were washed in water for 30-min prior to submission for resin embedding. Fixed and decalcified bone segments were rinsed in cacodylate buffer three times for 10 min each, and subjected to a secondary fixation for 1 h in a solution of 1% osmium tetroxide/1.5% potassium ferrocyanide in cacodylate buffer on ice for 1 h, rinsed in ultrapure water 3 times for 10 min each, and stained in an aqueous solution of 2% uranyl acetate for 1 h. The samples were then again washed in ultrapure water 3 times for 10 min each and dehydrated in a graded acetone series (50%, 70%, 90%, 100% ×2) for 10 min in each step. Tissues were then infiltrated with microwave assistance (Pelco BioWave Pro, Redding, CA) into LX112 resin and cured in an oven at 60 °C for 48 h.

2.2.2. Sample preparation protocol #2

Three datasets were generated with this protocol: (Dataset #3, Figs. 5, 7) C3H/HeJ proximal tibial metaphysis, 1592 serial electron micrographs, (Dataset #4, Fig. 6) C3H/HeJ tail vertebrae, 2433 serial electron micrographs and (Dataset #5, Fig. 8) C3H/HeJ tail vertebrae with immunostaining of tyrosine hydroxylase positive neurons, 2500 serial electron micrographs. An adult male C3H/HeJ mouse (Jackson Labs Stock: 000659) at 12-weeks of age was sedated with ketamine/xylazine and perfused with 10 mL saline followed immediately by 10 mL of fixative cocktail (0.15 M cacodylate buffer, 0.4% glutaraldehyde, 4.0% PFA, and 2.0% picric acid). The concentration of glutaraldehyde was decreased in the fixative to facilitate later immunostaining. The rest of the preparation is the same a 2.2.1. apart from the addition of 0.1 M imidazole to the osmium tetroxide staining solution. This was added to attempt better stabilization of the lipid-rich tail vertebrae samples. However, we did not observe any differences when compared to the samples without imidazole.

2.3. FIB-SEM scanning and analysis

Following resin curing, tissue blocks were mounted onto SEM pins with silver epoxy and surface polished with a diamond trim tool (Diatome Trim 90, Hatfield, PA). Blocks were then sputter coated with 10 nm of iridium (Leica ACE 600, Vienna, Austria) with rotation on a planetary stage to ensure uniform coating of the entire block. Following coating, samples were then loaded into a FIB-SEM (Zeiss Crossbeam 540, Oberkochen, Germany) and the cell of interest was located by

Table 1
Ultrastructural features of adipocytes. Previously published features of white [1–3,5,6], beige [2–4], and bone marrow adipocytes [10,11].

Ultrastructural feature	White adipocyte	Beige adipocyte	Bone marrow adipocyte
Cytoplasm	Thin rim around lipid	Evenly distributed around lipid and organelles	Thin rim around lipid
Lipid	Large central unilocular droplet, smaller lipid droplets in cytoplasm	Small lipid droplets dispersed throughout cytoplasm	Large central lipid globule with smaller fat globules noted in the peripheral cytoplasm
Surrounding matrix	Collagen-rich; adipocytes are “embraced” by a network of collagen fibers	Vastly reduced collagenous matrix relative to WAT	Lack of association with collagen, basal lamina positive for PAS and reticulin stains
Nucleus	Displaced toward periphery, crescent or triangular shape. Peripheral chromatin condensation along the nuclear membrane and in association with nucleoli.	Centrally located. Peripheral chromatin condensation with a central euchromatic area and nucleolus.	Displaced toward periphery, crescent or triangular shape. Peripheral chromatin condensation along the nuclear membrane and in association with nucleoli.
Mitochondria	Filamentous and spherical with rare, short, or gently wavy cristae	Numeous, large mitochondria with closely packed, straight cristae. Increased mitochondrial volume (3.7-fold *vs* WAT).	Dense, usually spherical mitochondria
Endoplasmic reticulum	Mostly smooth ER	Cisternae of rough ER	Some profiles of rough ER
Innervation	Unmyelinated nerve fiber with Schwann cells and ‘naked’ nerve fibers can be found adjacent to the membrane of some cells (~5% of adipocytes are innervated)	Every adipose cell was in close contact with one or more nonmyelinated nerve fibers (often 2, 3, or more contacts per cell) (100% of adipocytes are innervated)	Unknown
Vasculature	Adjacent to capillaries (~0.4 capilllaries/cell)	Adjacent to capillaries (~0.8 capillaries/cell)	Adjacent to sinusoidal endothelium
Contacts between adipocytes	Very limited (Loncar 1988 found only one direct contact between WAT adipocytes out of 2000 total cells)	Appearance of gap junction connections between adipocytes which connect nearly all cells to one another	Unknown

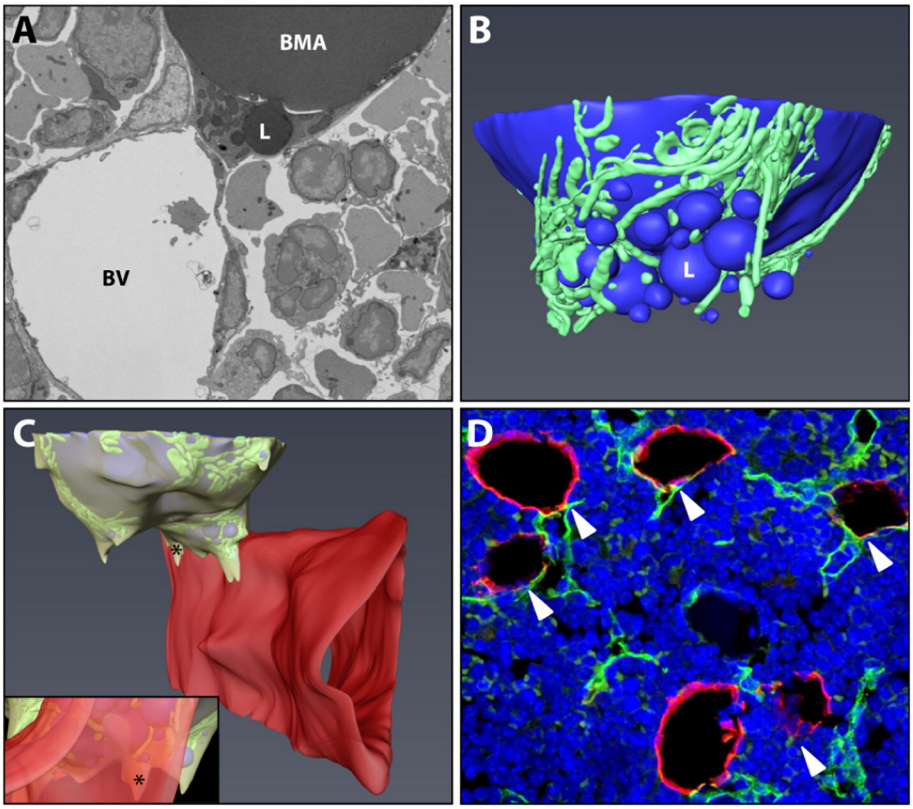

Fig. 1. Basic ultrastructure and vascular connections of the tibial bone marrow adipocyte. (A) The ultrastructure of a bone marrow adipocyte from the proximal tibial metaphysis of a wild type C57BL/6 J mouse was reconstructed from a FIB-SEM dataset containing 1329 independent images (Dataset #1). BMA = bone marrow adipocyte, BV = blood vessel, L = lipid droplet. (B) The reconstruction revealed a large lipid droplet and a multitude of smaller lipid droplets (blue). The *smaller lipid droplets* were enmeshed by a dense network of mitochondria (green). (C) The majority of the smaller lipid droplets were polarized toward a sinusoidal blood vessel (red). The adipocyte cytoplasm (yellow) was immediately adjacent to the endothelial cell of the blood vessel. Inset: view from the interior of the blood vessel toward the adipocyte. * = cytoplasm of BMA. Imaging location: C57BL/6 J mouse, proximal tibia. (D) Consistent with the EM study, immunohistochemical analysis of the bone marrow shows that perilipin positive bone marrow adipocytes (red) consistently make at least one connection with an endomucin positive blood vessel (green, arrowheads). DAPI in blue. Representative image from an 8-month-old male C57BL/6 J mouse (N = 3). See also Supplementary Video 1.

secondary electron imaging at 5 KeV. Once a region was identified, the sample was prepared using the ATLAS 3D nanotomography routine [19]. In short, a platinum pad was deposited on a 50 μm × 50 μm region of interest at 30 KeV and 15 nA. Three vertical lines for focus and stigmation correction and two angled lines for 3D-tracking were milled into the platinum pad at 100 pA, then filled with carbon at the same current to enhance the tracking/alignment marks, followed by an additional deposition of a protective carbon pad at 15 nA. A rough trench 50 μm deep was then milled at 30 nA and polished at 3 nA. Once polished, face detection, focusing, and 3D-tracking were all performed on the fiducial marks that were milled into the platinum pad. Imaging was performed at 1.75 KeV and 1.7 nA using the EsB detector with a grid voltage of 1000 V. The block was milled at a current of 700 pA with 20 nm slices and 2000 × 2000 pixel images were acquired at a resolution of 20 nm/pixel with a dwell of 7 μs and a line average of 3 for a total z-depth of approximately 40 μm. Images were then segmented and aligned using Amira 6 (Thermo Fisher, Hillsboro, OR).

2.4. Immunostaining

2.4.1. Frozen sections for fluorescent immunohistochemistry

Male 8-month old C57BL/6 J mice were perfused with 10% neutral-buffered formalin. Isolated femurs and tibiae were post-fixed for 24-h prior to decalcification in 14% EDTA, pH 7.4. Decalcified specimens were embedded in OCT mounting media and sectioned at 100 μm on a cryostat. Tissue sections were permeabilized for 10 min in 0.2% Triton-× 100 in phosphate buffered saline (PBS) and blocked for 1-h with 10% donkey serum in TNT buffer (0.1 M Tris-HCl pH 7.4, 0.15 M sodium chloride, 0.05% Tween-20). Primary antibody cocktail (1:400 perilipin, Progen GP29; 1:500 endomucin, BioLegend, 14-5851) was made in TNT buffer and incubated for 48-h at 4 °C. Secondary antibody cocktail (1:200 donkey anti-guinea pig Cy3; 1:200 donkey anti-rat Alexa 488; Jackson ImmunoResearch) was made in TNT buffer and incubated for 24-h at 4 °C. All washes between steps were performed in TNT buffer. Nuclei were counterstained with 1 μg/mL DAPI (Sigma, Saint Louis, MO, USA). Slides were imaged on an Olympus FV1200 confocal microscope.

2.4.2. Vibratome sections for immuno-electron microscopy

A vibratome was used to take 300 μm thick sections from the center of the C4 tail vertebrae prepared as in Section 2.2.2. The Vectastain® Elite ABC kit (Vector Laboratories) was used to stain the tyrosine hydroxylase positive sympathetic neurons for immuno-electron microscopy. Specifically, sections were washed in TNT buffer prior to quenching endogenous peroxidases with 0.3% hydrogen peroxide in PBS for 15-min. Sections were washed 3× in TNT after peroxidase inhibition prior to blocking for 2-h at room temperature in kit-specific reagents and subsequent incubation with primary antibody (1:1000 dilution in TNT, tyrosine hydroxylase, Millipore AB152) for 4-days at 4 °C. After washing 3× in TNT sections were incubated with the kit-provided secondary antibody overnight at 4 °C. After the secondary, sections were washed 3× in TNT and 1× in phosphate buffered saline (PBS) and then incubated in the kit-provided ABC reagent for 45 min. After washing 3× in PBS staining was visualized with metal enhanced-DAB (Metal Enhanced DAB Substrate Kit, Thermo Scientific). After a final

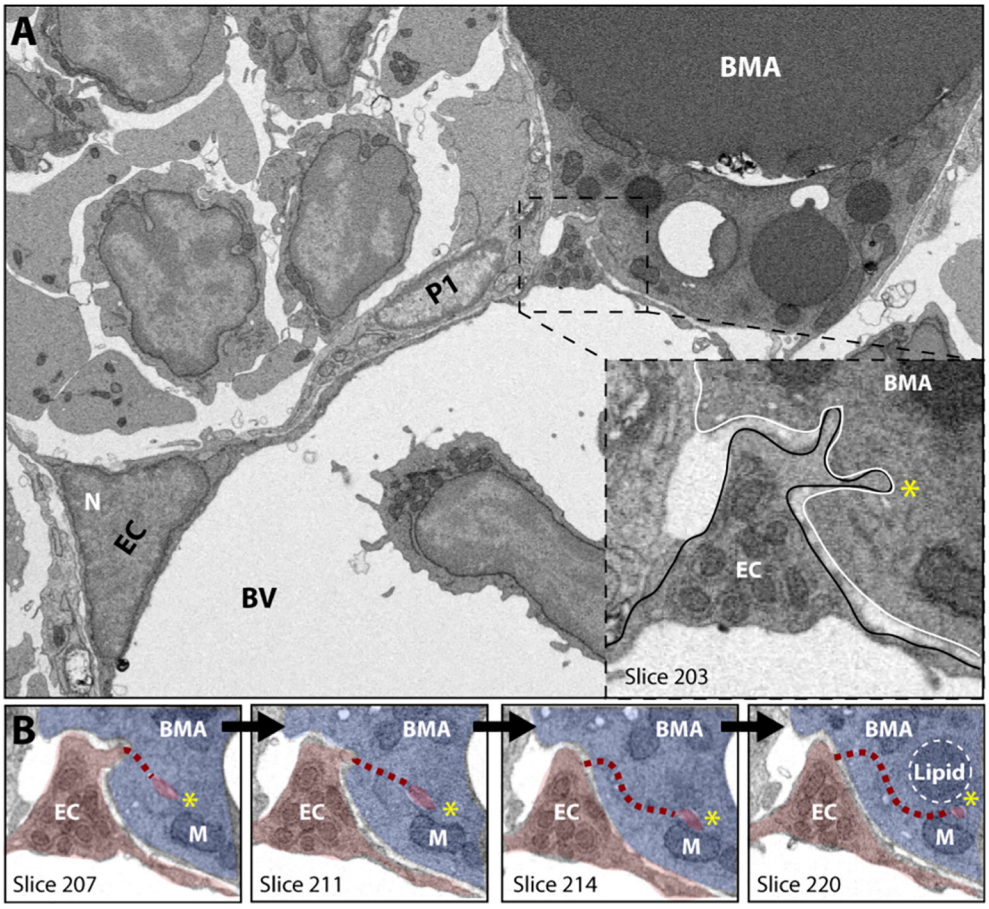

Fig. 2. Interactions between the vascular endothelial cell and the BMAT adipocyte. (A) The bone marrow adipocyte (BMA) is immediately adjacent to the endothelial cell-lined (EC) vascular sinusoid. Extravasated blood cells are noted in the lumen. The endothelial cell has a cytoplasmic swelling adjacent to the bone marrow adipocyte (boxed inset). The cytoplasm in the region of the swelling contains many organelles and extends cellular processes into the surface of the BMAT adipocyte. N = nucleus. BV = blood vessel. P1 = pericyte. (B) In this series of images we follow the endothelial cell process marked by the yellow asterisk (*) as one moves through the dataset from slice 207 to slice 220, a distance of approximately 0.25 μm. EC = endothelial cell, psuedocolored in red. BMA = bone marrow adipocyte, blue. M = mitochondria. The dashed line represents the path of the cell process which is currently out of frame. Imaging location: C57BL/6 J mouse, proximal tibia (Dataset #1).

wash, stained sections were returned to fixative at 4 °C and submitted for resin embedding, imaging and analysis as described above.

3. Results

3.1. The vascular niche of the bone marrow adipocyte

The BMA of the proximal tibia has an extensive network of spherical and filamentous mitochondria (Fig. 1). The mitochondria interweave around and between smaller lipid droplets, forming well-defined regions of cytoplasmic activity which are positioned spatially toward the sinusoid or the into regions of hematopoietic cells (Fig. 1B, C). Consistent with previous work in rabbits [10], we observed that BMAT adipocytes in the tibia of mice are closely associated with the sinusoidal vascular endothelium in C57BL/6 J and C3H/HeJ mice (Fig. 1 and data not shown). Indeed, based on immunohistochemical stains, it appears that every BMAT adipocyte in the proximal tibia has at least one connection to an endomucin-positive sinusoid (Fig. 1D).

In the area where the BMA meets the blood vessel, the vascular endothelial cell exhibits marked cytoplasmic swelling that is rich in organelles (Fig. 2A). This region of the endothelial cell extends membrane-covered cytoplasmic processes into the BMA - similar to fingers being pushed into the surface of balloon (Fig. 2B). The endothelial extensions can be observed to terminate adjacent to small triacylglycerol deposits within the BMAT adipocyte cytoplasm (Fig. 2B). It is also notable that in areas of decreased cell-cell interactions, a loose extracellular matrix can be observed between the BMAT adipocyte and the surface of the endothelial cell in C57BL/6 J (Supplementary Fig. 1) and C3H/HeJ mice (data not shown). This loose matrix is also present between endothelial cells and pericytes and between pericytes and the BMAT adipocyte.

3.2. Perivascular cells spatially restrict cell-cell interactions with BMAT adipocytes

In the tibial bone marrow of the B6 male mouse, pericyte-like cells enveloped the BMA with their flattened network of cytoplasmic extensions (Fig. 3). The pericytes themselves had large nuclei with an outer ring of condensed chromatin, prominent nucleoli, and loosely organized nuclear granules. The region of cytoplasm nearest the nucleus contained an extensive network of endoplasmic reticulum and rounded mitochondria with prominent cristae. Occasional mitochondria were also observed in the thinnest regions of the cytoplasmic extensions which encircled the BMAT adipocyte. Lipid inclusions were noted near the nucleus of one of the pericytes, on the side closest to the BMA (Fig. 3A). Of note, this type of perivascular cell lining of the BMA was not present in the tibial dataset from the C3H mouse (data not shown). Thus, the presence of perivascular cells is a selective feature of certain BMAT niches. When present, the pericytes appear to channel the BMAT adipocyte toward the vascular endothelial cells, seemingly serving to dock the adipocyte onto the blood vessel. The perivascular cell extensions also appear to restrict the cell-cell interactions of the mature BMAT adipocyte with surrounding cells.

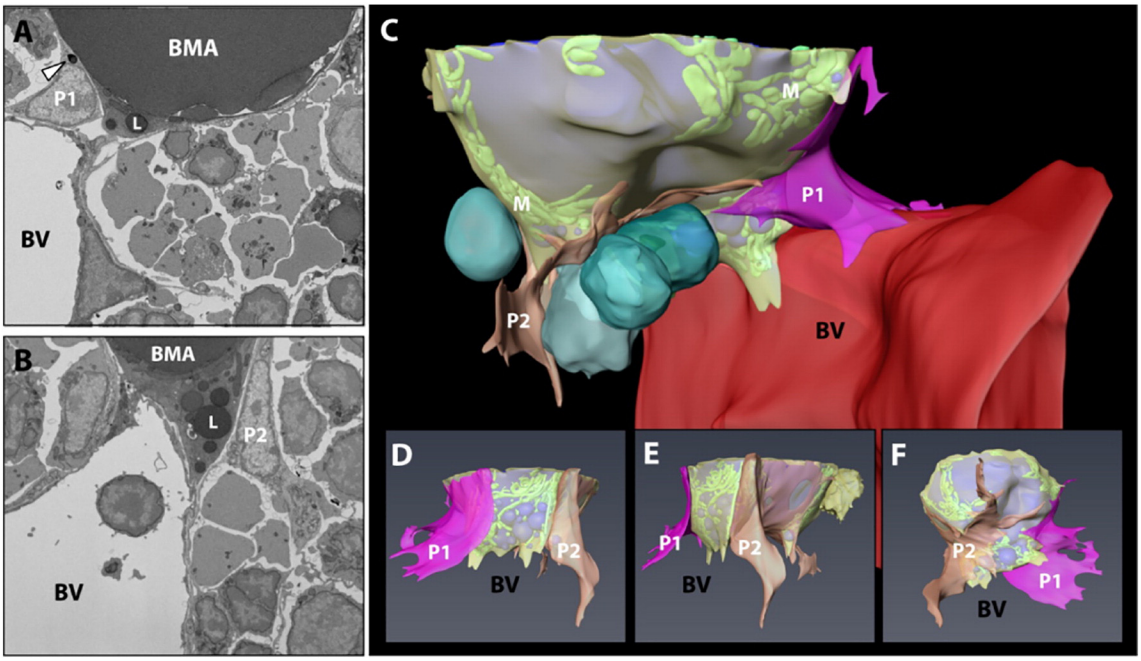

Fig. 3. Perivascular cell support of the BMAT adipocyte. (A, B) EM images of perivascular cell #1 and #2 (P1 and P2) around the BMAT adipocyte. These cells border the BMAT adipocyte and seem to dock it to the sinusoidal blood vessel (BV). The P1 perivascular cell contains lipid droplets (arrowhead). (C) Composite image of the adipocyte (lipid in blue, mitochondria "M" in green, cytoplasm in semi-transparent yellow), vascular sinusoid (red), perivascular cells (P1 in pink, P2 in orange) and blood cells (turquoise). (D, E, F) 3D reconstruction of perivascular cells #1 and #2 and the BMAT adipocyte with the blood vessel and hematopoietic cells removed. 'BV' denotes the spatial positioning of the blood vessel as the 3D image is rotated. BV = sinusoidal blood vessel. BMA = bone marrow adipocyte. L = lipid droplet. Imaging location: C57BL/6 J mouse, proximal tibia (Dataset #1).

3.3. BMAT adipocytes interact with hematopoietic cells within the bone marrow

As discussed above, in the B6 tibia we observed polarization of smaller BMAT lipid droplets toward the hematopoietic microenvironment. At first glance, it appeared that the BMAT adipocyte was interacting with a mononuclear blood cell of the developing erythroid lineage. However, upon closer examination of the 3D dataset, it became apparent that the BMA was actually interfacing with a phagocytic reticular cell, also known as a core macrophage of the erythroblast island (Fig. 4A, B). Erythroblast islands consist of central macrophage-like nurse cells that provide support for maturing erythroblasts and help to traffic them toward the sinusoids for later release of mature erythrocytes [20,21]. Maturing erythroblasts and anuclear erythrocytes (*aka.* reticulocytes) were commonly noted nearby the tibial BMAT adipocyte (Fig. 5A, B). The association between the BMAT adipocytes and erythroblast islands was also notable in the C3H mouse tibial BMAT microenvironment. In the C3H tibia dataset, the cells of the erythroblast island were more immature and had not yet lost their nuclei (Fig. 5C). The core phagocytic reticular cell was also unique in that it contained an extensive network of lipid droplets (Fig. 5C, D). It was associated with an impressive number of hematopoietic cells – 54 in total. Of these, 47 cells (87%) were nucleated erythroblasts, one cell had large granules consistent with that of a basophil, and six cells had smaller granules like those of the myeloid/granulocyte lineage (Supplementary Fig. 2). The cytoplasm of the core macrophage appeared to adhere directly to the BMAT adipocyte (Fig. 5C, D).

In addition to interactions with phagocytic reticular macrophages of the erythroblast islands, the BMA membrane was observed to be directly adjacent to that of maturing hematopoietic cells of the myeloid/granulocyte lineage in both B6 (Fig. 4C) and C3H mice (Fig. 5C). These interactions were relatively common. For example, the visible portion of the C3H BMA within the tibia (~30% of the cell) was directly associated with 20 individual blood cells, in addition to core macrophages from two erythroblast islands – which then extended to support many additional erythroblasts (blue cells in Figs. 4B and 5).

3.4. Characteristics of bone marrow adipocytes from regions of constitutive bone marrow adipose tissue in tail vertebrae

Using our current methods, the imaging quality in regions of the tail vertebrae where the BMAT adipocytes were confluent (*aka.* "constitutive" BMAs) was poor, allowing for only a cursory overview of the cells and their microenvironment (Fig. 6A). Specifically, the edges of the central lipid globules were covered by an electron dense precipitate, which obscured smaller regions of compressed cytoplasm (Fig. 6B). Larger cytoplasmic regions (*ex.* in areas of nuclei) could still be assessed. Based on what we could see, constitutive BMAT adipocytes have very large central lipid droplets, which compress their crescent-shaped nuclei to the periphery. In one of the cells, a large, secondary lipid body compressed the nucleus from the opposite direction, giving it a 'dumbell' like shape (Fig. 6B, dotted white line). Mitochondria were still present and a network of endoplasmic reticulum was occasionally observed (Fig. 6C). Very few intervening cells or structures were noted between the BMAT adipocytes. These findings were consistent in both B6 and C3H tail vertebrae datasets.

3.5. Characteristics of the BMAT adipocyte niche at the bone interface

Two regions of BMAT and bone lining cells were captured in our study. The first, in the C3H tibia, revealed extension of BMA cytoplasm toward an active osteoblast (Fig. 7, osteoblast in orange). In this region, the BMA cytoplasm was filled with sheets of endoplasmic reticulum and several small lipid droplets (Fig. 7, inset). Nearby, as observed in other regions (Figs. 4C, 5C) the BMA made direct contact with two hematopoietic cells (Fig. 7).

Images from the second BMA-bone interface, in the C3H tail vertebrae, captured an area of relatively quiescent-appearing osteoblasts atop collagen-rich osteoid and mineralized matrix (Fig. 8). This dataset was immunostained for tyrosine hydroxylase with subsequent precipitation of an electron dense, cobalt-nickel precipitate onto stained sympathetic nerve fibers. Prior to resin embedding we used confocal microscopy to

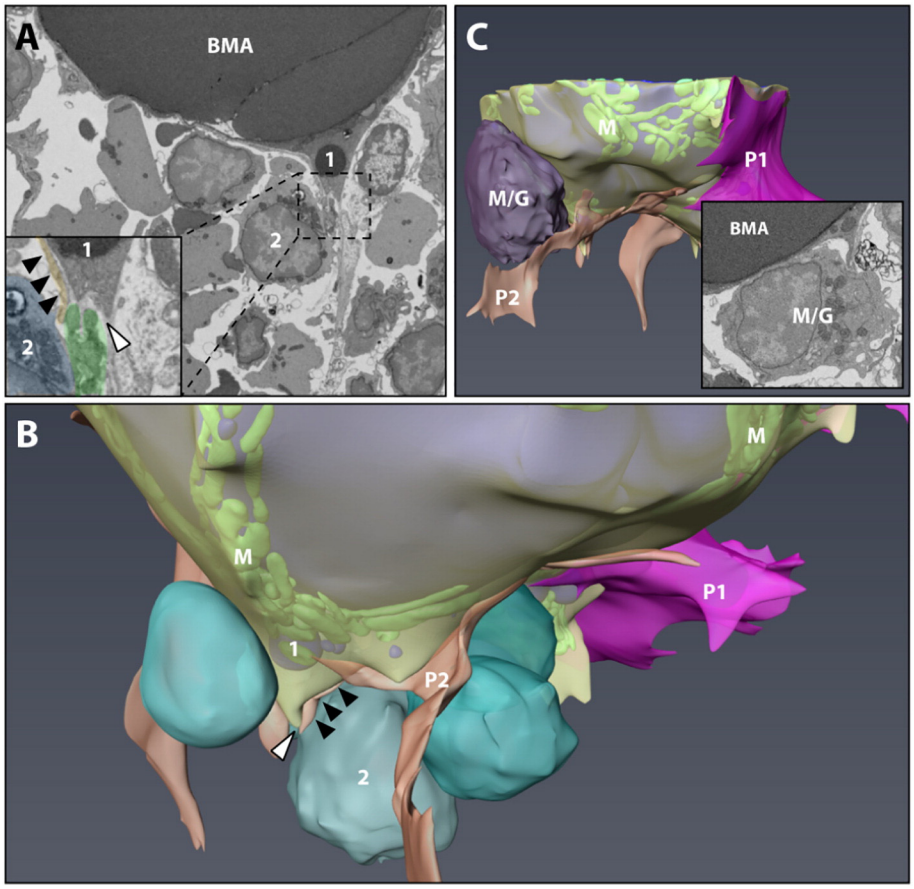

Fig. 4. The BMAT hematopoietic cell interface #1. (A, B) The tibial rMAT adipocyte was observed to interact with a phagocytic reticular cell (inset, green pseudocolor) adjacent to a mononuclear erythroblast (blue) with polarization of lipid droplets ('1') toward the hematopoietic microenvironment. Membrane remodeling by both the adipocyte and the erythroblast-supporting macrophage was noted at the site of interaction (white arrowhead). A perivascular cell extension was also quite prominent in this area (black arrowheads, orange). P1 = pericyte #1. P2 = pericyte #2. Composite image of the adipocyte is the same as Fig. 3 (lipid in blue, mitochondria 'M' in green, cytoplasm in semi-transparent yellow). (C) In an area without pericytes, the BMAT adipocyte interfaced directly with a large hematopoietic cell of the myeloid/granulocyte lineage (M/G). A small cytoplasmic extension with lipid droplets extended from the BMA to make contact with the blood cell (inset). See also Supplementary Video 2. Imaging location: C57BL/6 J mouse, proximal tibia (Dataset #1).

visualize these fibers in the whole thickness section of the tail vertebrae. Confocal analysis revealed dense, spiral shaped clusters of sympathetic neurons (Fig. 8A, arrowheads). The appearance was consistent with previous reports of perivascular sympathetic innervation in bone [22]. In select cases, these clusters of neurons sent delicate, branching terminal offshoots toward the bone surface and BMAT adipocytes (Fig. 8A, inset). Using the FIB-SEM, this interface was examined at 20 nm resolution. We confirmed that the sympathetic neurons formed a dense network around the arteriolar blood vessel (Fig. 8B, C). A small neuron also extended onto the surface of an adjacent BMA and terminated in the region of the BMA/bone interface (Fig. 8D). At this location, though collagen-rich osteoid was observed, the osteoblast lining cells appeared relatively flattened and quiescent (Fig. 8E). Between the osteoblast layer and the large BMA lipid globule, there was a third cell. The cytoplasm contained an elongated, crescent-shaped nucleus and was filled with many small lipid droplets, some of which appeared to be budding directly from the large unilocular droplet of the BMA (Fig. 8B, E). Based on our analysis of the full dataset, this seemed like it could be an extension of the BMA itself. However, due to some distortion in the dataset, this point remains a bit unclear. Regardless, this clearly demonstrates that smaller lipid bodies tend to cluster near to the osteoblast layer and in regions of sympathetic innervation.

4. Discussion

This work reveals several local contexts at the vascular, hematopoietic, and osteogenic interfaces in which BMAs exist and function. The proximity of the BMAT adipocyte to surrounding cells likely contributes to its physiology, as evidenced, for example, by polarization of triacylglycerol deposits and cellular organelles toward key interfaces. This may be comparable to small lipid droplets which accumulate within peripheral WAT adipocytes [23]. These deposits are generally located near the cell membrane and provide a larger surface area for lipases, facilitating rapid increases in both the rate and magnitude of lipolysis [23]. In BMAT adipocytes, localization of lipid droplets to the cell surface could facilitate the egress and spatial partitioning of free fatty acids from BMAs to target cells through lateral transfer across defined interfacial planes of adjacent membranes [5], contributing to its putative role as a local regulator of energy partitioning.

4.1. Bone marrow adipocytes and hematopoiesis

The reach of the BMAT adipocyte is extensive. Based on the C3H proximal tibia dataset, we estimate that one BMA was capable of interacting with in excess of 100 hematopoietic cells through both direct cell-cell contact and indirect signals *via* binding with the core macrophage of erythroblast islands [20,21]. Bone marrow generates 400 to 500 billion cells per day in adult humans (0.5 to 1.5 billion in mice) – regenerating approximately half of the circulating cellular content (reviewed in Nombela-Arrieta and Manz [24]). Thus, the incorporation of a cellular energy reserve into the hematopoietic niche seems remarkably logical. Indeed, this is evolutionarily conserved. Adipocytes have been present within the hematopoietic marrow since the relegation of

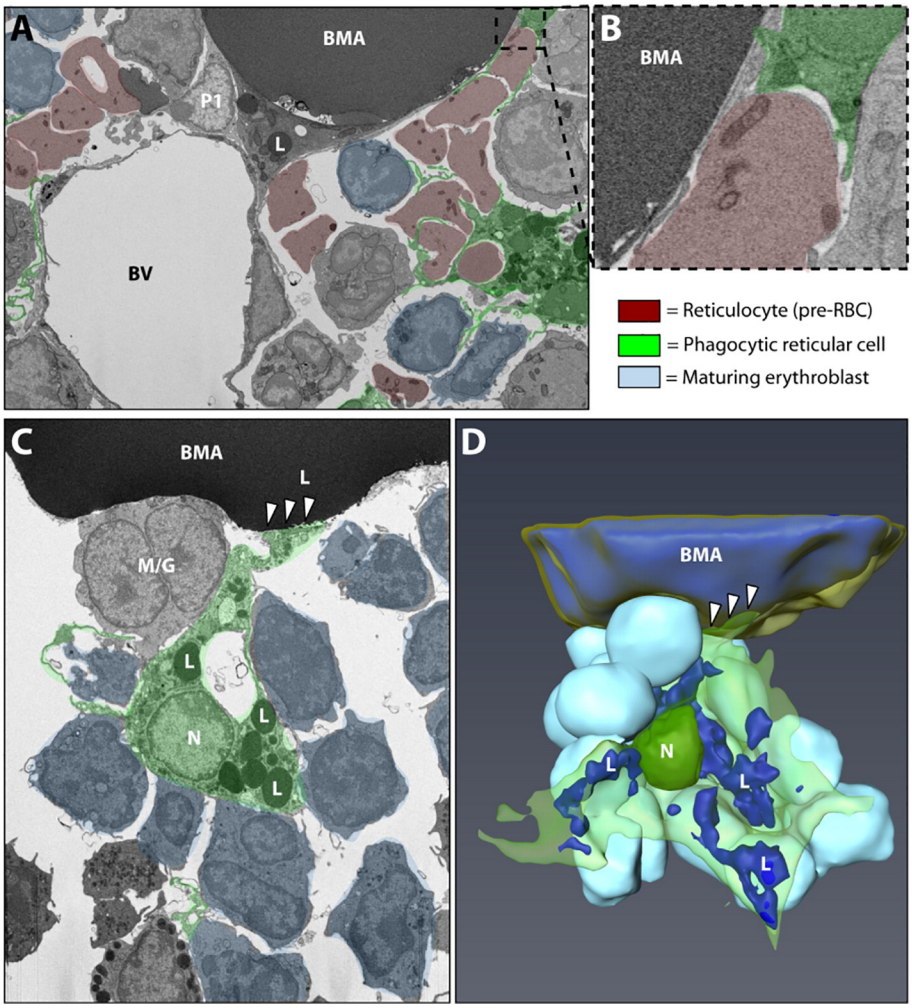

Fig. 5. Interactions between BMAT adipocytes and erythroblast islands. (A) Electron microscopic image of the bone marrow adipocyte (BMA) microenvironment showing the core phagocytic reticular cell/macrophage of the erythroblast island (psuedocolored green). Reticulocytes, immature red blood cells which lack nuclei but retain some cellular organelles, are pseudocolored in red. Maturing erythroblasts which have not yet lost their nuclei are in light blue. In this dataset, the core macrophage was filled with cellular debris due to phagocytosis of the reticulocyte nuclei. (B) Magnified inset shows the close association between the phagocytic reticular cell and the BMA. Imaging location: C57BL/6 J mouse, proximal tibia (panel A, B; Dataset #1). (C) In the C3H dataset, another phagocytic reticular cell was observed. However, this time the associated erythroblasts had not yet lost their nuclei. Instead of being filled with debris, the core macrophage contained an extensive network of small lipid droplets (L). The macrophage extended a process which appeared to be attached to the BMA (white arrowheads). A cell of the myeloid/granulocyte lineage was also noted to be immediately adjacent to the BMA. (D) 3D reconstruction of the BMA and erythroblast island in panel C. Imaging location: C3H/HeJ mouse, proximal tibia (panel C, D; Dataset #3). See also Supplementary Video 2.

hematopoiesis to the skeleton in bony fishes, amphibians and reptiles (reviewed in Craft and Scheller [25]). Lymph nodes also have a unique perinodal adipocyte reserve which supports lymphogenesis and, like BMAT, is disassociated from systemic energy demand [26,27].

Our imaging implies that BMAs are spatially positioned to influence both erythropoiesis and myelopoiesis. The clinical importance of this was recently emphasized. Specifically, disruption of the BMAT niche during acute myeloid leukemia resulted in impaired myelo-erythroid maturation [28]. Restoration of BMAs with a PPARγ agonist helped to resolve this defect in hematopoiesis [28]. Erythrocytes develop and mature within erythroblast islands [21]. However, despite their energy demands, immature islands are often distant from bone marrow sinusoids [20]. Instead, they migrate toward the sinusoid as erythrocyte maturation occurs [20]. Thus, when present in the niche, BMAT adipocytes may help to shuttle energy to distant, immature erythroid islands, supporting the maturation of red blood cells. In times of acute demand, BMAT lipid could also be quickly liberated to provide fuel for excess red blood cell synthesis. This is consistent with previous studies in experimental animals which showed rapid decreases in BMAT adipocyte size during reactive red blood cell formation after phenylhydrazine-induced anemia or severe blood loss [17,29]. This may also explain the results of a recent report showing that treatment with erythropoietin, a potent stimulant of erythrocyte maturation, markedly reduced BMAT in chow and high-fat diet fed mice, and inhibited the increase in BMAT with high-fat feeding [30]. Future characterization of this BMA/hematopoietic interface is needed to identify BMAT-derived factors, for example SCF [31], which contribute to blood cell production. Conversely, more work is needed to define signals of hematopoietic origin which regulate BMA formation and function.

4.2. Marrow adipocytes and bone formation

The complexities of the relationship between BMAT and bone have been reviewed elsewhere [32]. In addition to extensive interactions with hematopoietic cells, we observed polarization of BMA lipid droplets and cytoplasmic organelles toward vascular endothelial cells and areas of osteoblasts. Our work provides three key insights about the relationship between BMAT and bone. First, active osteoblasts may receive protein or lipid signals from nearby BMAT adipocytes, as evidenced by polarization of regions of endoplasmic reticulum and

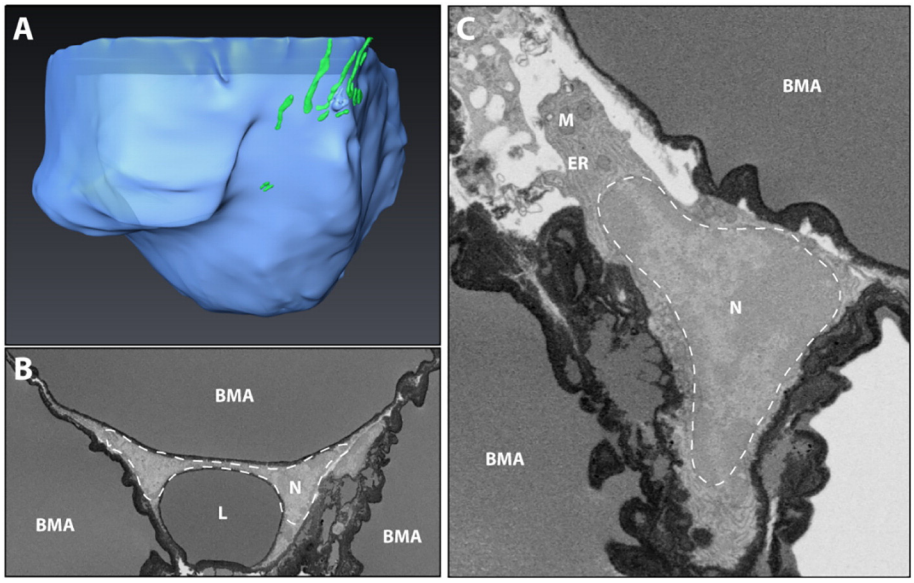

Fig. 6. Constitutive bone marrow adipocytes in the tail vertebrae. (A) 3D reconstruction of a BMAT adipocyte from the tail vertebrae in a region of dense, confluent adipocytes – also referred to as 'constitutive' bone marrow adipose tissue. Lipid in blue, mitochondria in green. Imaging location: C57BL/6 J mouse, tail vertebrae (Dataset #2). (B, C) In the C3H dataset, a dark precipitate was observed around the lipid droplets. In panel B three adipocytes converge. The nucleus (N) of the top adipocyte is compressed by a secondary lipid droplet (L) into a dumbbell-like shape. In panel B, the nucleus has a more conventional triangle/crescent-like morphology. The nucleus is surrounded by prominent areas of endoplasmic reticulum (ER) and occasional mitochondria (M). Imaging location: C3H/HeJ mouse, tail vertebrae (Dataset #4).

triacylglycerol deposits. Second, BMAs may provide fatty acids directly to bone lining cells. Third, the sympathetic nervous system may function to coordinate interactions at the BMAT/bone interface.

4.3. The bone marrow adipocyte progenitor

In 1978, Biermann et al. described the ultrastructure of the various subtypes of reticulum cells in the bone marrow [33]. These were defined as the network of cells whose processes build a framework upon which all other activity in the bone marrow proceeds. They have also been referred to as stromal cells. Type I fibrous reticulum cells were defined as having extensive cellular processes with filaments of 4 to 8 nm in diameter that are characteristically located near the blood sinus in the bone marrow. By contrast, type II fibrous reticulum cells had serpentine filaments of 10 nm in diameter and a multiplicity of interdigitating cell processes. Type II fibrous reticulum cells often contained neutral fat bodies and reversible conversion to adipocytes was assumed [33]. This description is consistent with the lipid-containing perivascular cell observed in Fig. 3 and matches current literature which pinpoints pericytic progenitors as a key source of bone marrow adipocytes [34,35].

4.4. Innervation and vascularization of the BMAT niche

As previously reported [10], we also observed that BMAs are closely associated with the sinusoidal vasculature. This location could facilitate efficient uptake and storage of fatty acids from the circulation and

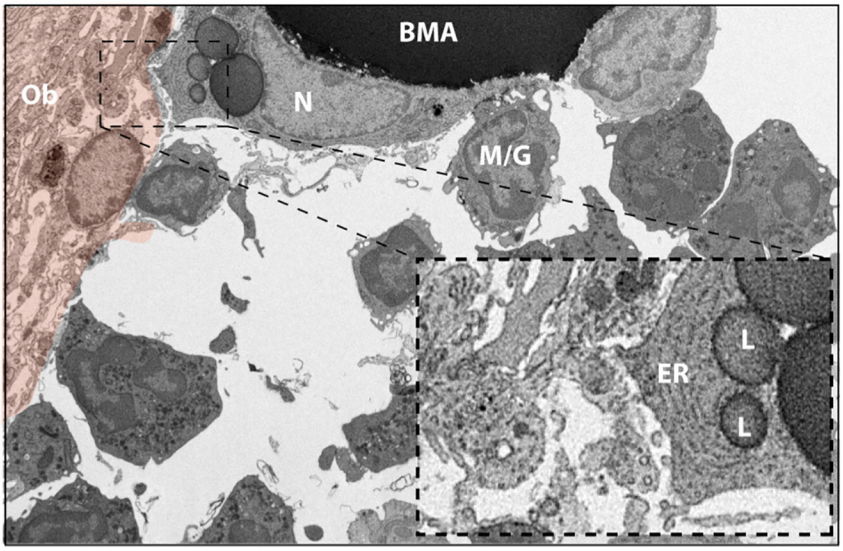

Fig. 7. The BMA and bone interface #1. The tibial bone marrow adipocyte (BMA) extends a cell process toward an active osteoblast-appearing cell (orange pseudocolor). The BMA nucleus (N) is crescent shaped with a ring of condensed heterochromatin and an associated nucleolus. The BMA cell extension contains prominent endoplasmic reticulum (ER) and lipid droplets (L) and is near to many smaller vesicles in the extracellular space (inset). The BMA is also associated with an adjacent blood cell of the myeloid/granulocyte lineage (M/G). Several additional granulocytes are noted in the surrounding bone marrow. Imaging location: C3H/HeJ mouse, proximal tibia (Dataset #3).

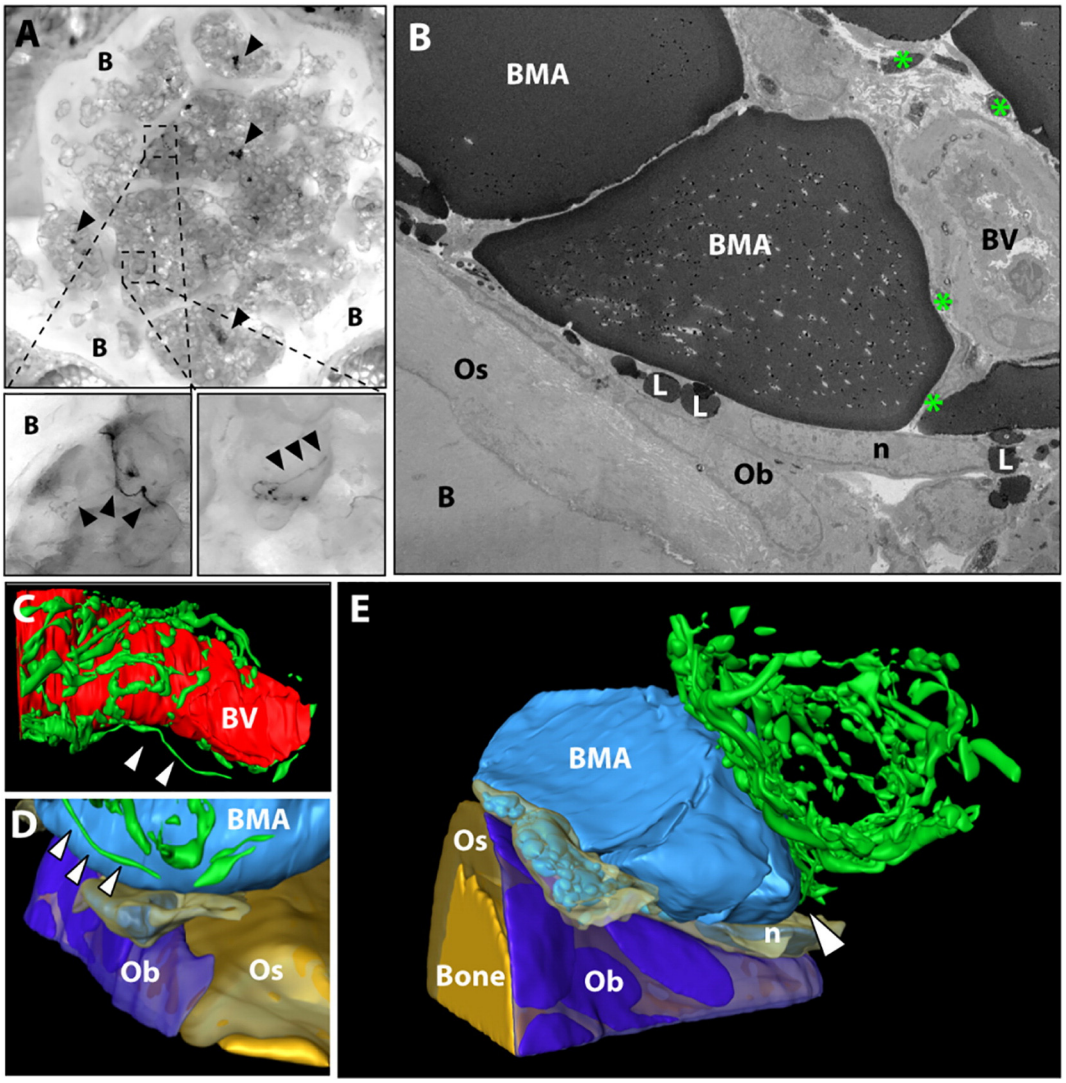

Fig. 8. The BMA and bone interface #2. (A) Immunostaining with cobalt-nickel precipitation for analysis of tyrosine hydroxylase positive sympathetic nerves (arrowheads) in tail vertebrae bone (B). Dark black precipitate highlights clusters of neurons in the vertebral space and delicate branches which extend onto the bone marrow adipocyte (BMA) and toward the bone interface (black arrowheads). (B) 2D image from a FIB-SEM dataset showing nerves (green *) near the bone surface which closely approximate an arteriolar blood vessel (BV). The flattened, crescent shaped nucleus (n) of a lipid-droplet (L) filled cell is present atop a flattened osteoblast (Ob). The osteoblast sits on layers of collagen-rich osteoid (Os) and mineralized bone (B). (C) The tysosine hydroxylase positive sympathetic nerves form a dense mesh around the artery. (D) A single nerve fiber extends from the mesh toward the surface of the BMA and terminates in the region of the osteoblast/BMA interface. (E) The osteoblast surface is immediately adjacent to a lipid filled cell with nucleus 'n' which may represent a cytoplasmic extension of the larger, unilocular BMA or a separate lipid-filled reticular cell. Imaging location: C3H/HeJ mouse, tail vertebrae + immunostain (Dataset #5).

subsequent directed release to cells within the bone marrow. This type of pattern is exemplified in Figs. 1 and 2, where smaller lipid droplets are polarized both toward the vascular sinusoid and toward an area of hematopoietic cell interaction. By contrast, in Fig. 8 we observed BMAT adipocytes adjacent to an artery. Unlike the endothelial niche, features of the arterial niche function to maintain quiescence of local cells [36]. Polarization of BMA lipid droplets toward the arterial space was not prominent. Instead, a sympathetic neuron branched from the vaso-regulatory neural meshwork to terminate in a region of osteoid synthesis. A lipid droplet-filled cell and an adjacent adipocyte were also observed, suggesting that neural stimulation may help to coordinate the BMAT and bone interface at some sites.

4.5. Differences between proximal tibia and tail vertebrae

In addition to occurring in areas of hematopoietic bone marrow, BMAs also form in areas of the skeleton that are relatively devoid of hematopoiesis [25]. So, what role could these cells play and are they distinct from the BMAT adipocytes which interface with hematopoietic cells? The concept of 'regulated' and "constitutive" BMAT adipocytes has been discussed previously, however, their implications for skeletal and systemic homeostasis remain unclear [12,37]. Our work confirms that in regions of constitutive BMAs, the adipocytes are packed closely with one another with very little intervening between them. Though mitochondria, endoplasmic reticulum, and small triacylglycerol deposits were observed in the cytoplasm, overall, there appeared to be less than what was present in the tibial BMAT adipocytes.

4.6. Limitations

These results are based on the analysis of 8821 electron micrographs from five independent FIB-SEM datasets across mice of two different strains (B6 and C3H). Thus, though we are confident in the qualitative results, the extent to which each niche feature exists quantitatively within a pool of BMAT adipocytes remains unknown. In addition, we were unable to examine the membrane architecture (*i.e.* presence of

caveolae), the presence of ribosomes on the endoplasmic reticulum, or the phospholipid covering that is characteristic of adipocyte lipid droplets [38]. Higher resolution electron micrographs or alternate techniques such as cryo-EM are needed to overcome these limitations. Lastly, we are still working to develop protocols to promote optimal sample stabilization and image quality in regions of confluent adipocytes. Despite these limitations, this work provides a robust overview of the unique cellular and ultrastructural features of the BMA and its niche.

5. Conclusions

These images provide a unique opportunity to visualize the native bone marrow adipocyte within its skeletal niche. In addition to confirming previous results from 2D EM studies, our images strongly imply that BMAs actively participate in physiologic energy partitioning and signaling within the skeletal microenvironment. This appears to be key for interactions of BMAT adipocytes with cells of the hematopoietic and osteogenic lineages. In addition, we've identified a subpopulation of BMAs that is innervated by the sympathetic nervous system. The main limitation of this study is its focus on healthy rodent adipocytes. Future work is needed to extend these results in humans and to determine whether maladaptation of BMAT with disease leads to relevant ultrastructural changes in the BMA niche.

Supplementary data to this article can be found online at https://doi.org/10.1016/j.bone.2018.01.020.

Acknowledgments

This work was supported by the National Institutes of Health, grants R00-DE024178 and U01-DK116317 (E.L.S.). Funding for this project was provided by the Children's Discovery Institute of Washington University and St. Louis Children's Hospital (Grant no: CDI-CORE-2015-505, J.A.J.F, M.S.J., and C.S.C.) and from the Foundation for Barnes-Jewish Hospital (Grant no: 3770, J.A.J.F. and M.S.J.). Lastly, completion of this work was supported by a fellowship from the Washington University career center (H.R.) and BioSURF summer research fellowship (S.P.).

References

[1] J. Carpentier, A. Perrelet, L. Orci, Morphological changes of the adipose cell plasma membrane during lipolysis, J. Cell Biol. 72 (1) (Jan 1977) 104–117.
[2] D. Lončar, L. Bedrica, J. Mayer, B. Cannon, J. Nedergaard, B.A. Afzelius, et al., The effect of intermittent cold treatment on the adipose tissue of the cat, J. Ultrastruct. Mol. Struct. Res. 97 (1–3) (Oct 1986) 119–129.
[3] D. Loncar, B.A. Afzelius, B. Cannon, Epididymal white adipose tissue after cold stress in rats. I. Nonmitochondrial changes, J. Ultrastruct. Mol. Struct. Res. 101 (2–3) (1988 Dec) 109–122.
[4] D. Loncar, Convertible adipose tissue in mice, Cell Tissue Res. 266 (1) (Oct 1991) 149–161.
[5] E.J. Blanchette-Mackie, R.O. Scow, Lipolysis and lamellar structures in white adipose tissue of young rats: lipid movement in membranes, J. Ultrastruct. Res. 77 (3) (Dec 1981) 295–318.
[6] L. Napolitano, The differentiation of white adipose cells. An electron microscope study, J. Cell Biol. 18 (Sep 1963) 663–679.
[7] J. Wu, P. Boström, L.M. Sparks, L. Ye, J.H. Choi, A.H. Giang, et al., Beige adipocytes are a distinct type of thermogenic fat cell in mouse and human, Cell 150 (2) (Jul 20 2012) 366–376.
[8] T.B. Waldén, I.R. Hansen, J.A. Timmons, B. Cannon, J. Nedergaard, Recruited vs. nonrecruited molecular signatures of brown, "brite," and white adipose tissues, Am. J. Physiol. Endocrinol. Metab. 302 (1) (Jan 1 2012) E19–31.
[9] S. Lim, J. Honek, Y. Xue, T. Seki, Z. Cao, P. Andersson, et al., Cold-induced activation of brown adipose tissue and adipose angiogenesis in mice, Nat. Protoc. 7 (3) (Mar 1 2012) 606–615.
[10] M. Tavassoli, Marrow adipose cells. Ultrastructural and histochemical characterization, Arch. Pathol. 98 (3) (Sep 1974) 189–192.
[11] M. Tavassoli, Ultrastructural development of bone marrow adipose cell, Acta Anat. (Basel) 94 (1) (1976) 65–77.
[12] E.L. Scheller, W.P. Cawthorn, A.A. Burr, M.C. Horowitz, O.A. MacDougald, Marrow adipose tissue: trimming the fat, Trends Endocrinol. Metab. 27 (6) (Jun 2016) 392–403.
[13] E.L. Scheller, C.J. Rosen, What's the matter with MAT? Marrow adipose tissue, metabolism, and skeletal health, Ann. N. Y. Acad. Sci. 1311 (Apr 2014) 14–30.
[14] M.J. Devlin, A.M. Cloutier, N.A. Thomas, D.A. Panus, S. Lotinun, I. Pinz, et al., Caloric restriction leads to high marrow adiposity and low bone mass in growing mice, J. Bone Miner. Res. 25 (9) (Sep 2010) 2078–2088.
[15] W.P. Cawthorn, E.L. Scheller, B.S. Learman, S.D. Parlee, B.R. Simon, H. Mori, et al., Bone marrow adipose tissue is an endocrine organ that contributes to increased circulating adiponectin during caloric restriction, Cell Metab. 20 (2) (Aug 5 2014) 368–375.
[16] M.A. Bredella, P.K. Fazeli, K.K. Miller, M. Misra, M. Torriani, B.J. Thomas, et al., Increased bone marrow fat in anorexia nervosa, J. Clin. Endocrinol. Metab. 94 (6) (Jun 2009) 2129–2136.
[17] M. Tavassoli, Marrow adipose cells. Histochemical identification of labile and stable components, Arch. Pathol. Lab. Med. 100 (1) (Jan 1976) 16–18.
[18] A. Bathija, S. Davis, S. Trubowitz, Bone marrow adipose tissue: response to acute starvation, Am. J. Hematol. 6 (3) (1979) 191–198.
[19] H.G. Lo, R.U. Jin, G. Sibbel, D. Liu, A. Karki, M.S. Joens, et al., A single transcription factor is sufficient to induce and maintain secretory cell architecture, Genes Dev. 31 (2) (Jan 15 2017) 154–171.
[20] T. Yokoyama, T. Etoh, H. Kitagawa, S. Tsukahara, Y. Kannan, Migration of erythroblastic islands toward the sinusoid as erythroid maturation proceeds in rat bone marrow, J. Vet. Med. Sci. 65 (4) (Apr 2003) 449–452.
[21] D. Manwani, J.J. Bieker, The erythroblastic island, Curr. Top. Dev. Biol. 82 (2008) 23–53.
[22] D.B. Mach, S.D. Rogers, M.C. Sabino, N.M. Luger, M.J. Schwei, J.D. Pomonis, et al., Origins of skeletal pain: sensory and sympathetic innervation of the mouse femur, Neuroscience 113 (1) (2002) 155–166.
[23] R.M. Smith, L. Jarett, Surface structure changes of rat adipocytes during lipolysis stimulated by various lipolytic agents. A scanning electron microscopic study, J. Cell Biol. 84 (1) (Jan 1980) 57–65.
[24] C. Nombela-Arrieta, M.G. Manz, Quantification and three-dimensional microanatomical organization of the bone marrow, Blood Adv. 1 (6) (Feb 14 2017) 407–416.
[25] C.S. Craft, E.L. Scheller, Evolution of the marrow adipose tissue microenvironment, Calcif. Tissue Int. 100 (5) (Jul 1 2016) 1–15.
[26] C.A. Mattacks, C.M. Pond, Interactions of noradrenalin and tumour necrosis factor alpha, interleukin 4 and interleukin 6 in the control of lipolysis from adipocytes around lymph nodes, Cytokine 11 (5) (May 1999) 334–346.
[27] C.M. Pond, C.A. Mattacks, The source of fatty acids incorporated into proliferating lymphoid cells in immune-stimulated lymph nodes, Br. J. Nutr. 89 (3) (Mar 2003) 375–383.
[28] A.L. Boyd, J.C. Reid, K.R. Salci, L. Aslostovar, Y.D. Benoit, Z. Shapovalova, et al., Acute myeloid leukaemia disrupts endogenous myelo-erythropoiesis by compromising the adipocyte bone marrow niche, Nat. Cell Biol. 19 (11) (Nov 2017) 1336–1347.
[29] A. Bathija, S. Davis, S. Trubowitz, Marrow adipose tissue: response to erythropoiesis, Am. J. Hematol. 5 (4) (1978) 315–321.
[30] S. Suresh, J.C. Alvarez, C.T. Noguchi, Paper: erythropoietin eliminates increased bone marrow adiposity and alters bone features in obese mice [Internet]Available from: American Society of Hematology, https://ash.confex.com/ash/2017/webprogram/Paper102008.html 2017.
[31] B.O. Zhou, H. Yu, R. Yue, Z. Zhao, J.J. Rios, O. Naveiras, et al., Bone marrow adipocytes promote the regeneration of stem cells and haematopoiesis by secreting SCF, Nat. Cell Biol. 19 (8) (Aug 2017) 891–903.
[32] A.G. Veldhuis-Vlug, C.J. Rosen, Mechanisms of marrow adiposity and its implications for skeletal health, Metab. Clin. Exp. 67 (Feb 2017) 106–114.
[33] A. Biermann, D. Graf von Keyserlingk, Ultrastructure of reticulum cells in the bone marrow, Acta Anat. (Basel) 100 (1) (1978) 34–43.
[34] B.O. Zhou, R. Yue, M.M. Murphy, J.G. Peyer, S.J. Morrison, Leptin-receptor-expressing mesenchymal stromal cells represent the main source of bone formed by adult bone marrow, Cell Stem Cell 15 (2) (Aug 7 2014) 154–168.
[35] T. Mizoguchi, S. Pinho, J. Ahmed, Y. Kunisaki, M. Hanoun, A. Mendelson, et al., Osterix marks distinct waves of primitive and definitive stromal progenitors during bone marrow development, Dev. Cell 29 (3) (May 12 2014) 340–349.
[36] Y. Kunisaki, I. Bruns, C. Scheiermann, J. Ahmed, S. Pinho, D. Zhang, et al., Arteriolar niches maintain haematopoietic stem cell quiescence, Nature 502 (7473) (Oct 31 2013) 637–643.
[37] E.L. Scheller, C.R. Doucette, B.S. Learman, W.P. Cawthorn, S. Khandaker, B. Schell, et al., Region-specific variation in the properties of skeletal adipocytes reveals regulated and constitutive marrow adipose tissues, Nat. Commun. 6 (Aug 6 2015) 7808.
[38] T. Fujimoto, R.G. Parton, Not just fat: the structure and function of the lipid droplet, Cold Spring Harb. Perspect. Biol. 1 (Mar 2011) 3(3).